JBMR®

A Novel HR-pQCT Image Registration Approach Reveals Sex-Specific Changes in Cortical Bone Retraction With Aging

Bert van Rietbergen,[1] Emmanuel Biver,[2] Thierry Chevalley,[2] Keita Ito,[1] Roland Chapurlat,[3] and Serge Ferrari[2]

[1]Orthopaedic Biomechanics, Department of Biomedical Engineering, Eindhoven University of Technology, Eindhoven, The Netherlands
[2]Division of Bone Diseases, Geneva University Hospitals and Faculty of Medicine, Geneva, Switzerland
[3]INSERM UMR 1033, Université de Lyon, Lyon, France

ABSTRACT

During aging, changes in endosteal and periosteal boundaries of cortical bone occur that differ between men and women. We here develop a new procedure that uses high-resolution peripheral quantitative CT (HR-pQCT) imaging and 3D registration to identify such changes within the timescale of longitudinal studies. A first goal was to test the sensitivity of the approach. A second goal was to assess differences in periosteal/endosteal expansion over time between men and women. Rigid 3D registration was used to transform baseline and all follow-up (FU) images to a common reference configuration for which the region consisting of complete slices (largest common height) was determined. Periosteal and endosteal contours were transformed to the reference position to determine the net periosteal and endosteal expansion distances. To test the sensitivity, images from a short-term reproducibility study were used (15 female, aged 21 to 47 years, scanned three times). To test differences between men and women, images from a subset of the Geneva Retirees Cohort were used (248 female, 61 male, average age 65 years, 3.5 and 7 years FU). The sensitivity study indicated a least significant change for detecting periosteal/endosteal expansion of 41/31 microns for the radius and 17/26 microns for the tibia. Results of the cohort study showed significant net endosteal retraction only in females at the radius and tibia after 3.5 years (38.0 and 38.4 microns, respectively) that further increased at 7 years FU (70.4 and 70.8 microns, respectively). No significant net periosteal changes were found for males or females at 7 years. The results demonstrate that it is possible to measure changes in endosteal contours in longitudinal studies within several years. For the investigated cohort, significant endosteal retraction was found in females but not in males. Whether these changes in cortical geometry are related to fracture risk remains to be investigated in larger cohorts © 2021 The Authors. *Journal of Bone and Mineral Research* published by Wiley Periodicals LLC on behalf of American Society for Bone and Mineral Research (ASBMR).

KEY WORDS: AGING; BONE QCT/μCT; CLINICAL TRIALS; OSTEOPOROSIS; BIOMECHANICS

Introduction

During aging, changes in endosteal and periosteal boundaries of cortical bone occur that differ between men and women. In women, endosteal resorption takes place, leading to a reduction of cortical area and a reduction of the second moment of area, hence, bone strength, whereas in men, the endosteal resorption is compensated for by periosteal expansion, leading to little change in cortical area and some increase in the second moment of area, hence, bone strength.[1–5] Such changes are typically attributed to hormonal changes during aging; in particular, estrogen loss after menopause in women is known to lead to increased endosteal resorption and impaired periosteal bone apposition and thus may explain the more severe effect in women than in men.[6,7] In the metaphyseal region, this endosteal resorption is typically manifested as trabecularization of the inner cortical region.[5] However, other conditions and drug treatment can also lead to changes in endosteal and periosteal geometry. Chronic inflammatory diseases, such as rheumatoid arthritis, are associated with an accelerated endosteal bone resorption and compensatory periosteal bone formation.[7–9] Hyperparathyroidism has been reported to lead

to increased trabecularization of the endosteal boundary.[10] Antiresorptive drugs, such as bisphosphonates and denosumab, can reduce cortical porosity[11–14] and thus reduce the endosteal expansion by trabecularization of the cortex in metaphyseal regions. Also, anti-sclerostin drugs, such as romosozumab, have been reported to have an effect on endocortical bone formation and cortical thickness.[15] Finally, parathyroid hormone (PTH) treatments have been reported to accelerate intracortical remodeling as well as endosteal remodeling with a net positive balance between bone formation and resorption on the endosteal surface.[16–19] Thus, a quantitative assessment of changes in periosteal and endosteal boundaries during a longitudinal (drug) study can potentially provide new information about the progression of the disease and the efficacy of its treatment.

The rate at which the periosteal and endosteal boundaries change, however, is very low. Reported values for periosteal apposition rates during aging are in the range of 10 to 25 microns/year, whereas those for endosteal resorption are in the range of 20 to 58 microns/year, depending on sex, site, age, and treatment.[6,20] Because clinical CT or peripheral quantitative CT (pQCT) imaging modalities typically have a resolution that is ≥0.25 mm, it would take a decade or more to detect such small periosteal/endosteal changes in longitudinal studies.

With the introduction of high-resolution peripheral quantitative CT (HR-pQCT) devices, images with a resolution of 82 or 61 microns (depending on model type) are possible for the distal radius and distal tibia.[21,22] At least in theory, this makes it possible to detect changes in periosteal/endosteal boundaries at these sites within 2 to 3 years, which is a feasible period for follow-up studies. To detect such changes, however, first a reliable approach for the definition of cortical boundaries is required. Fully automated segmentation algorithms have been developed in earlier studies to detect the periosteal and endosteal boundaries, and it has been shown that these enable a reproducible and objective assessment of the cortical boundaries.[23,24] Second, a precise registration of baseline (BL) and follow-up (FU) images is needed. The 1-dimensional (area matching) registration procedure, which is part of the standard HR-pQCT clinical workflow, will not be suitable because due to the somewhat wedged shape of the distal radius and tibia, any periosteal expansion/retraction will lead to a longitudinal shift that will obscure changes in periosteal diameter (Fig. 1).[25] This can be solved by using a 3D rigid registration method that focuses on the trabecular bone microstructure.[26–28]

In this study, we develop a procedure that uses HR-pQCT imaging, automatic boundary detection, and 3D registration to detect changes in periosteal/endosteal boundaries in clinical follow-up studies over multiple time points. A first goal was to test the sensitivity of the approach. To do so, data obtained from a short-term reproducibility study for which no significant changes in periosteal/endosteal boundaries should be detected was used. A second goal was to assess differences in periosteal/endosteal expansion over time between men and women in a larger cohort of subjects during normal aging. Subjects were included at retirement, and follow-up scans were available at 3.5 and 7 years thereafter.

Materials and Methods

Algorithm development for detection of periosteal/endosteal expansion

The algorithm developed here consists of three steps. All these steps were implemented using IPLFE version 2.03 (Scanco Medical AG, Brüttisellen, Switzerland).

Creating masks of the cortical and cancellous bone compartments

Masks of the cortical bone compartment were derived from the periosteal and cancellous bone contours. The periosteal contour was generated as part of the standard clinical workflow and can be obtained using a semi-automatic snake algorithm or using a fully automatic algorithm.[23] The cancellous bone contour used here was generated as part of the HR-pQCT extended cortical analysis.[23,24] A mask of the total bone region was obtained first by setting the value of voxels within the periosteal contour to their maximum value. Next, a mask of the cancellous compartment was made by setting all voxels within the cancellous contour to their maximum value. Finally, a mask of the cortical compartment was obtained by subtracting the cancellous mask from the total bone mask.
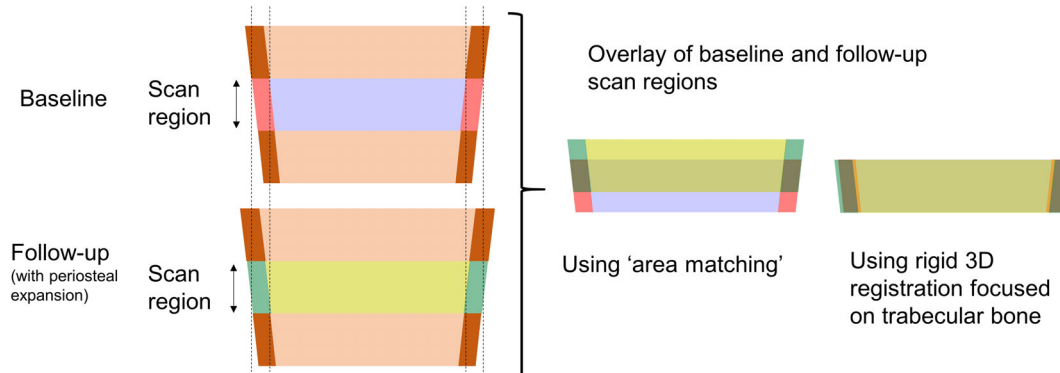
Fig 1. Schematic overview of the overlay of a baseline (BL) and follow-up (FU) image in case of periosteal expansion. When using the area matching algorithm, the periosteal expansion will lead to a longitudinal shift of the FU image, thus obscuring the expansion. Using 3D rigid image registration focused on the trabecular bone microstructure, a correct positioning can be obtained that will reveal the periosteal expansion.
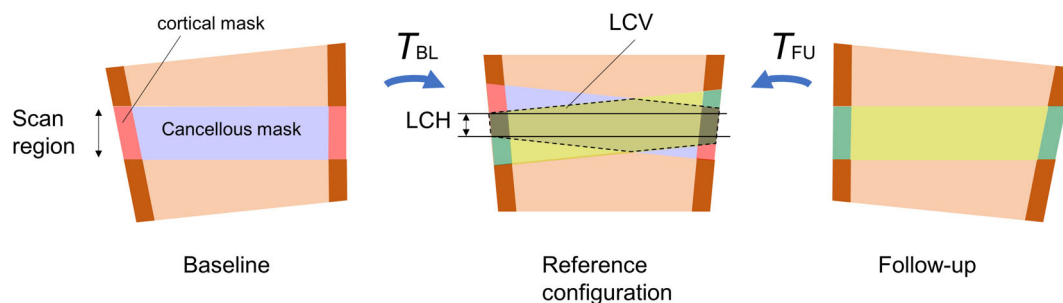
Fig 2. Cortical and cancellous masks of the BL (left) and FU (right) images are transformed to a common reference configuration (middle). After transformation, it is possible to calculate the largest common volume (LCV) of the cancellous and cortical masks (indicated here by the dashed lines as well as the largest common height (LCH) of the masks (indicated by the parallel lines). The LCH represent the number of slices in the reference configuration for which complete information is available for the transformed BL and all FU images.

Determination of the largest common value (LCV) and the largest common height (LCH) of the baseline and follow-up measurements

3D rigid image registration was used to find the transformation of the baseline (BL) and all follow-up (FU) images to a common reference position. This reference position was defined as the position halfway between the BL and the first FU image (Fig. 2). The reason for defining a separate reference position, eg, rather than taking the BL image as the reference position, is twofold: first, it maximizes the largest common height (see below), and second, it implies that all masks will be transformed, including the BL masks. As transformation involves interpolation and binarization, this avoids that some masks are not interpolated while others are. The reference position was determined by first performing a 3D rigid registration of the FU image to the BL image to obtain the translation and rotation values. The 3D registration algorithm uses a pre-registration based on fitting the center of mass, followed by the actual registration that was performed using a simplex algorithm with the image correlation coefficient as the objective function.[27] To speed up the process and avoid registration errors, the registration was performed in three steps. In the first step, the image resolution was reduced by a factor of 8, in the second step by a factor of 4, and in the last step registration was based on the full resolution image. Linear interpolation was used during the 3D registration process and to transform the final images. The resulting Euler angles and translation vector found for registering the FU image to the BL image were divided by 2, and a transformation matrix T was calculated based on these new values. The baseline image was then transformed to the reference position by applying a transformation $T_{BL} = T^{-1}$ and acted as the reference model to which all FU images were registered. For each of the FU images, a two-step 3D rigid registration was performed to this reference model. In the first step, the full bone section (cortical and cancellous compartment) was used for the registration, while in the second step, starting from the transformation found in the first step, only the cancellous region of the FU image was registered to the cancellous region of the reference model. In this way, a transformation matrix T_i was found for each FU image i. Based on the transformation matrices thus found, the masks defining the cortical and cancellous compartments were transformed to the reference position (Fig. 2). The LCV then was defined as the voxels in the reference configuration that are both in the transformed BL and all transformed FU total bone masks. The LCV mask can

be back-transformed to the original measurement images for accurate measurement of morphological parameters in the LCV without having to interpolate the actual images.[25–27] However, this was unnecessary in this study because all measurements related to the periosteal/endosteal expansion are performed on the transformed masks and do not require further morphological parameter evaluations.

In a final step, the LCH of all measurements was determined. The LCH is defined as the largest number of slices in the reference position containing complete information of the BL and all FU images (Fig. 2). This LCH was calculated automatically by separately transforming only the top and bottom slice of the total mask to the reference position and then finding the first and the last slice in the reference position in which no remnants of the top and bottom slice were present.

To get the most accurate results, all image registration was performed using the gray-level images. To quantify the quality of the registration, binary images in which the bone tissue was segmented were transformed and overlaid as well using the same transformation matrices. Segmented images were obtained as part of the standard clinical workflow and involve Laplace-Hamming filtering and thresholding.[21] From the overlay of the segmented images, the number of overlapping bone voxels was expressed as a percentage of the total number of bone voxels in the overlay image (ie, a value of 100% would indicate perfect overlap). This overlap was calculated only for the LCV of the registered area (ie, the cancellous bone region).

Quantification of the periosteal/endosteal expansion/retraction

All further quantification was done using the LCH of the cortical and cancellous compartment masks transformed to the reference configuration. The voxels of the cortical mask of the BL image were assigned a value of 1, while those of the cancellous mask were assigned a value of 2. For each of the FU images, the voxels of the cortical compartment were assigned a value of 4, while those of the cancellous compartment were assigned a value of 8. Next, the BL masks and the mask of one of the FU masks were added. For the LCH, this results in a total of eight different values, each of which indicates a unique change of the cortical boundaries (Fig. 3). For example, a voxel value of 4 indicates a voxel available in the FU cortical mask but not in the BL cortical mask, hence, indicating periosteal expansion. A value of 5 indicates a voxel common to the cortical mask at BL and FU, while a value of 9 indicates
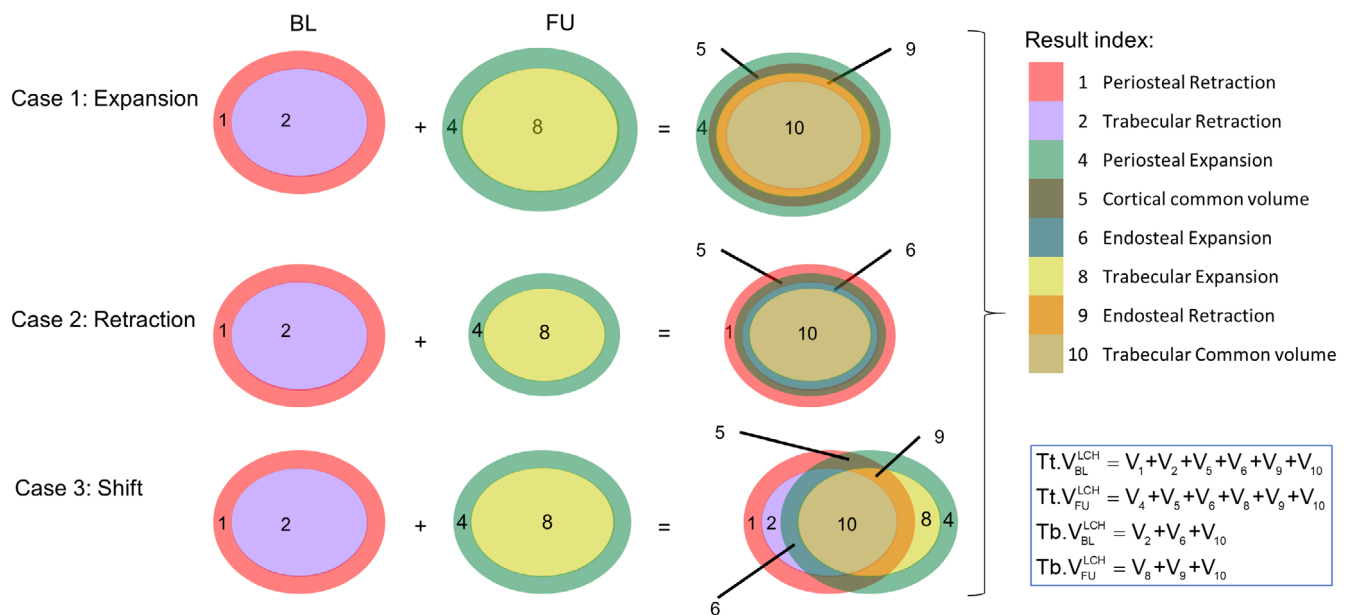
Fig 3. Generation of compartment overlay images. At baseline (BL), the cortical compartment is assigned a value of 1 and the cancellous compartment a value of 2. At follow-up (FU), these values are 4 and 8, respectively. After addition of the images, only eight different values can exist, each of which indicates a specific displacement of compartment boundaries as indicated in the index. The baseline and follow-up volumes can be calculated as shown in the right-bottom box, where $Tt.V_{BL}^{LCH}$ represents the LCH baseline total volume, $Tt.V_{FU}^{LCH}$ the LCH follow-up total volume, $Tb.V_{BL}^{LCH}$ the LCH baseline trabecular volume, and $Tb.V_{FU}^{LCH}$ the LCH follow-up trabecular volume. Parameter V_1 refers to the volume of voxels in the overlayed image with a value of 1, V_2 to the volume of voxels with a value of 2, etc.

a voxel that at BL was in the cortical mask but at FU in the cancellous mask, hence, endosteal retraction. With the terminology used here, expansion at both the endosteal and periosteal side is defined as a movement in outward direction relative to the mid of the cortical bone ring, hence, an increase in cortical bone volume. The volumes with a voxel value of 2 in the added image represent a situation where the periosteal boundary retracts into what at baseline was the trabecular compartment, while volumes with a voxel value of 8 represent a situation where the trabecular compartment expands outside the original periosteal border. Although these cases are expected to be rare with normal bone remodeling, they are kept here to ensure a correct calculation of endosteal expansion/retraction in case of shifting boundaries or growth where these cases can exist (Fig. 3).

As the common cortical volume and the common trabecular volume (case 5 and 10) do not directly reflect changes related to expansion or retraction, these were not further considered here. To correct the expansion/retraction results for differences in bone size and LCH height, volumes calculated for the periosteal expansion/retraction were divided by the baseline LCH total (ie, periosteal) surface $Tt.S_{BL}^{LCH}$, while those related to endosteal expansion/retraction were divided by the baseline LCH trabecular (ie, endosteal) surface $Tb.S_{BL}^{LCH}$. This effectively changes the expansion/retraction volumes to an average expansion/retraction distance. An overview of the parameters thus determined and their acronyms is given in Table 1.

Finally, a net periosteal expansion distance (Net.Per.Exp) was calculated as the ratio of the change of the total bone volume (the volume within the periosteal boundary) over the BL periosteal surface:

Table 1. Parameters Representing Periosteal/Endosteal Expansion/Retraction

Voxel value	Description	Acronym
4	Periosteal expansion	Per.Exp
1	Periosteal retraction	Per.Ret
6	Endosteal expansion	End.Exp
9	Endosteal retraction	End.Ret
2	Trabecular retraction	Tb.Ret
8	Trabecular expansion	Tb.Exp
	Net periosteal expansion	Net.Per. Exp
	Net endosteal expansion	Net.End. Exp
	Net periosteal expansion without 3D registration	Net.Per. Exp*
	Net endosteal expansion without 3D registration	Net.End. Exp*

All parameters have units of microns. The voxel values relate to those listed in Fig. 3.

$$Net.Per.Exp = \frac{Tt.V_{FU}^{LCH} - Tt.V_{BL}^{LCH}}{Tt.S_{BL}^{LCH}} = \frac{V_4 + V_8 - V_1 - V_2}{Tt.S_{BL}^{LCH}} \quad (1)$$

with $Tt.V_{BL}^{LCH}$ the total volume within the LCH at baseline, $Tt.V_{FU}^{LCH}$ the total volume within the LCH, and V_i the volume of voxels with value i as defined in Fig. 3. Similarly, a net endosteal expansion distance (Net.End.Exp) was calculated as:

Table 2. Mean Values, Standard Deviations (SD), and Least Significant Change (LSC) of the Periosteal/Endosteal Expansion/Retraction Distances at the Radius and Tibia

	Snake algorithm			Autocontouring		
	Average	(SD)	LSC	Average	(SD)	LSC
			Radius			
Per.Exp	34.4	(13.1)	32.0	30.3	(14.0)	34.9
Per.Ret	26.5	(6.4)	18.1	23.3	(7.0)	18.7
End.Ret	31.9	(12.2)	24.0	31.7	(12.5)	25.0
End.Exp	27.2	(8.0)	18.3	27.6	(8.0)	18.1
Tb.Exp	0.0	(0.0)	0.0	0.0	(0.0)	0.0
Tb.Ret	0.0	(0.0)	0.1	0.0	(0.0)	0.0
Net.Per.Exp	7.9	(16.4)	40.6	7.1	(17.2)	43.1
Net.End.Exp	−4.7	(16.5)	31.0	−4.1	(16.6)	31.6
Net.Per.Exp*	NA			−5.2	(126)	237.2
Net.End.Exp*	NA			−8.8	(164)	303.9
			Tibia			
Per.Exp	30.2	(10.9)	15.7	24.3	(10.7)	16.7
Per.Ret	28.9	(10.4)	13.8	23.7	(10.8)	14.6
End.Ret	34.4	(12.4)	13.9	34.3	(12.5)	13.4
End.Exp	36.2	(9.7)	21.8	36.2	(9.5)	21.8
Tb.Exp	0.0	(0.0)	0.0	0.0	(0.0)	0.0
Tb.Ret	0.0	(0.0)	0.0	0.0	(0.0)	0.0
Net.Per.Exp	1.3	(7.7)	16.9	0.6	(8.6)	17.6
Net.End.Exp	1.8	(11.5)	26.4	1.9	(11.6)	25.9
Net.Per.Exp*	NA			1.9	(43.2)	99.3
Net.End.Exp*	NA			−2.4	(58.4)	130.9

Values are in units of microns.
*Indicates results without the 3D registration.

$$Net.End.Exp = \frac{Tb.V_{BL}^{LCH} - Tb.V_{FU}^{LCH}}{Tb.S_{BL}^{LCH}} = \frac{V_6 + V_2 - V_9 - V_8}{Tb.S_{BL}^{LCH}} \quad (2)$$

With $Tb.V_{BL}^{LCH}$ the trabecular volume within the LCH at baseline, $Tb.V_{FU}^{LCH}$ the trabecular volume within the LCH at FU and V_i the volume of voxels with value i. Note that with these net parameters, a positive value indicates expansion in outward direction, hence, an increase in cortical bone volume, while a negative value indicates retraction, hence, cortical bone loss.

To investigate the improvement that can be obtained by using the 3D registration procedure, the Net.Per.Exp and the Net.End.Exp were also calculated based on the change in total volume (Tt.V) and trabecular volume (Tb.V) as obtained from the advanced cortical analysis for the full set of 110 slices without using 3D registration:

$$Net.Per.Exp^* = \frac{Tt.V_{FU} - Tt.V_{BL}}{Tt.S_{BL}} \quad (3)$$

$$Net.End.Exp^* = \frac{Tb.V_{BL} - Tb.V_{FU}}{Tb.S_{BL}} \quad (4)$$

with $Tt.S_{BL}$ and $Tb.S_{BL}$ the total (periosteal) bone surface and trabecular (endosteal) bone surface, respectively, for the full 110 slices.

Sensitivity study

Images for the sensitivity study were taken from an earlier study.[21] In summary, a total of 15 women were included (aged 21 to 47 years). The protocol was approved by an independent Ethics Committee, and all patients gave written informed consent before participation. For each subject, the distal radius and distal tibia were scanned three times on three different days within 1 month. HR-pQCT images were made at the distal radius and tibia using standard clinical settings at a resolution of 82 microns (XtremeCT, Scanco Medical). The periosteal contours were generated first as part of the default clinical workflow using a snake algorithm and were manually corrected if needed. In a second analysis, contours were generated using an autocontouring algorithm without any manual corrections.[23] In both cases, the endosteal contours were generated fully automatically without any manual corrections.[23,24]

For each subject, the LCH of the three measurements was determined using the algorithm described above. For the LCH region, the periosteal/endosteal expansion/retraction parameters as in Table 1 were determined for each of the two repeated measurements, taking the first measurement as the baseline.

Based on the three repeated measurements, the least significant change (LSC) is calculated. This LSC sets a threshold on measured changes that needs to be exceeded to ensure (at a certain level of confidence) that the measured changes exceed the precision errors of a technique.[29] To calculate the LSC, first for each individual subject the standard deviation $SD(P)$ of the repeated measures of parameter P was calculated, with P being one of the defined expansion/retraction distances (all parameters in Table 1). Next, the LSC of the parameters was determined for the case of one BL and one FU measurement as in[29–31]:

$$LSC = Z\sqrt{2}SD(P)_{RMS} = 2.77SD(P)_{RMS} \qquad (5)$$

with Z, the Z-score which was set to a 95% confidence interval ($Z = 1.96$) and SD(P)RMS the root-mean-square average of the 15 SD(P) values.

The Net.Per.Exp* and Net.End.Exp* were not calculated for the snake algorithm-derived contours because the calculation of Tt.V using the advanced cortical analysis is based on automatically generated contours. Analyses were performed separately for the distal radius and tibia.

Cohort study

To test differences in periosteal/endosteal expansion between men and women, images taken from a subset of the GERICO cohort (Geneva Retirees Cohort http://www.isrctn.com/ISRCTN11865958) were used.[32] Participants in this cohort (male and female) were included at the age of 65 years at BL. The subjects used here (female: $n = 248$; male: $n = 61$) were selected from the larger GERICO cohort based on the requirement that a FU image was available at 3.5 years ± 1 year or 7 years ± 1 year or at both time points for the radius or tibia. For each subject, the distal radius and distal tibia were scanned using standard clinical settings at a resolution of 82 microns (XtremeCT, Scanco Medical). Periosteal contours were generated as part of the default clinical workflow, which included manual correction if needed, using a snake algorithm. The endosteal contours were generated using an autocontouring algorithm without any manual corrections.[23] Further details of the study are described elsewhere.[32] The study protocol received the approval from the Geneva University Hospitals' Ethics Committee, and all participants provided written informed consent.

Results were calculated only for FU measurements for which at least a 50% overlap was found with BL during registration of the segmented images, a threshold that was based on the results of the sensitivity study. To investigate the effect of this threshold on the results, a threshold of 40% and 60% was also applied. For each individual subject, the net periosteal and net endosteal expansion was calculated using Eqns 1 and 2. Next, the average values were calculated per time point and per group (male/female).

As the data were found to be not normally distributed, a Kruskal–Wallis one-way ANOVA test was performed to test differences in the expansion/retraction parameters between male, female, and the sensitivity study participants (for the latter using the average of the two repeated measurements). In case of significant differences, Dunn's pairwise post hoc test was used and significance vales were adjusted by the Bonferroni correction to adjust for multiple comparisons. A Wilcoxon

signed rank test was performed to test if there were significant differences in these parameters at the two follow-up time points.

To compare the results with parameters typically reported in earlier HR-pQCT studies, standard cortical parameters were also calculated for the full images (110 slices) without registration using the analyses as described in Burghard and colleagues.[24] These parameters included the total volume (Tt.V), trabecular volume (Tb.V), and cortical thickness (Ct.Th) and were calculated at baseline and the two follow-up time points. As the data was found to be not normally distributed, a Friedman two-way ANOVA by ranks test was performed to test if there were significant differences in these parameters over time. In case of significant differences, Dunn's pairwise post hoc test was used and significance values were adjusted by the Bonferroni correction to adjust for multiple comparisons.

All statistical analyses were performed using SPSS v25 (IBM Corp., Armonk, NY, USA).

Results

Sensitivity study

For all subjects, the 3D registration provided adequate results as confirmed by visual inspection. The average (SD) percentage overlap of the registered segmented images was 65% (5.8%) for the radius and 71% (5.4%) for the tibia. Based on these numbers, a 50% threshold was defined for the cohort study, which represents the average −2.5 SD value for the radius. Whereas the full size of all images was 110 slices, the average size of the LCH in the reference position was 99 (SD = 5) slices for the radius and 93 (SD = 12) slices for the tibia. The average and LSC values as calculated according to Eq. 5 for the different parameters are shown in Table 2. When calculating the Net.Per.Exp* and Net.End.Exp* for the full 110 slices, much higher standard deviations were found, resulting in LSC values that can be around 10 times higher for the radius and about 6 times higher for the tibia. For this reason, these measures were not further considered.

Cohort study

The total number of radius scans available at each time point and site and the percentage overlap (%OL) between BL and FU images after 3D registration is shown in Table 3. As expected, the overlap within the LCV region between BL and FU images was less than for the sensitivity study, and the overlap was slightly better for the 3.5 years FU than for the 7 years FU, indicating structural changes over time. After applying the 50% threshold on the registration overlap, the number of scans available for the distal radius analysis was reduced by

Table 3. The Number of Scans Available at Each Time Point and the Average Overlap %OL With Standard Deviation (SD) Between Baseline (BL) and Follow-up (FU) Images Within the LCV Region

	Radius				Tibia			
	Female		Male		Female		Male	
	3.5 years	7 years	3.5 years	7 years	3.5 years	7 years	3.5 years	7 years
n	208 [135]	212 [130]	54 [49]	56 [43]	225 [215]	237 [218]	56 [53]	57 [53]
%OL	53.9 (8.4) [58.9 (5.4)]	52.8 (8.9) [58.5 (5.2)]	59.5 (7.4) [60.8 (6.4)]	56.6 (8.4) [59.8 (6.4)]	63.9 (7.7) [64.8 (6.5)]	63.6 (7.9) [65.1 (6.2)]	64.1 (7.6) [65.2 (6.0)]	63.2 (7.3) [64.5 (5.7)]

The numbers after applying the 50% overlap threshold are shown in square brackets.
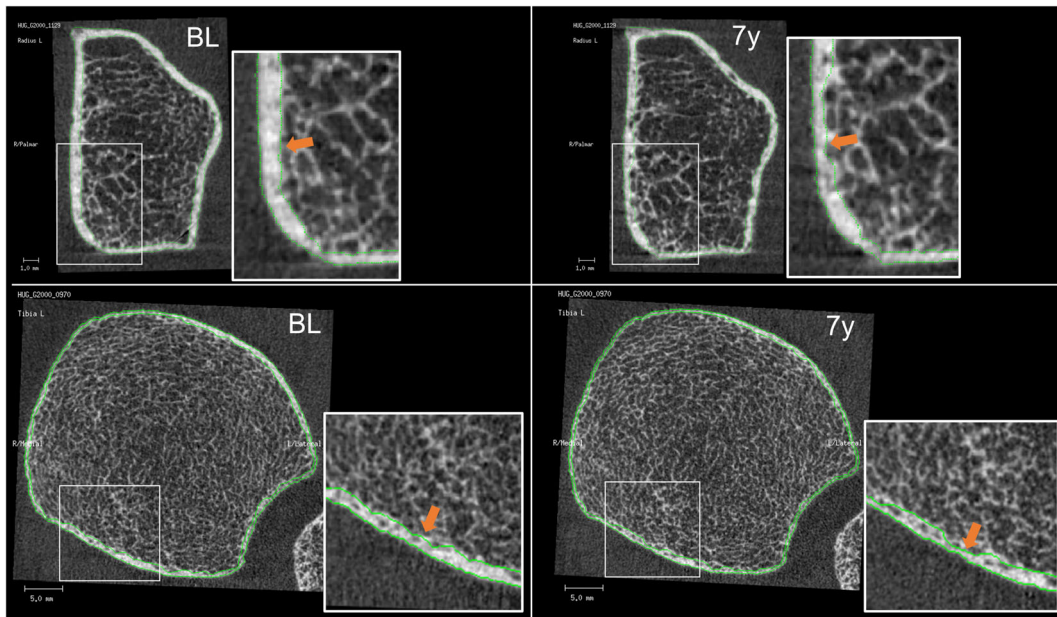
Fig 4. Examples of a typical female cross-sectional image of the registered baseline (BL) and 7-year follow-up (7y) image for the radius (top) and tibia (bottom). The green lines indicate the periosteal and endosteal contours. The arrows indicate regions where cortical trabecularization occurs, leading to endosteal retraction.

1 Periosteal Retraction
2 Trabecular Retraction
4 Periosteal Expansion
5 Cortical Common Volume
6 Endosteal Expansion
8 Trabecuar Expansion
9 Endosteal Retraction
10 Trabecular Common Volume
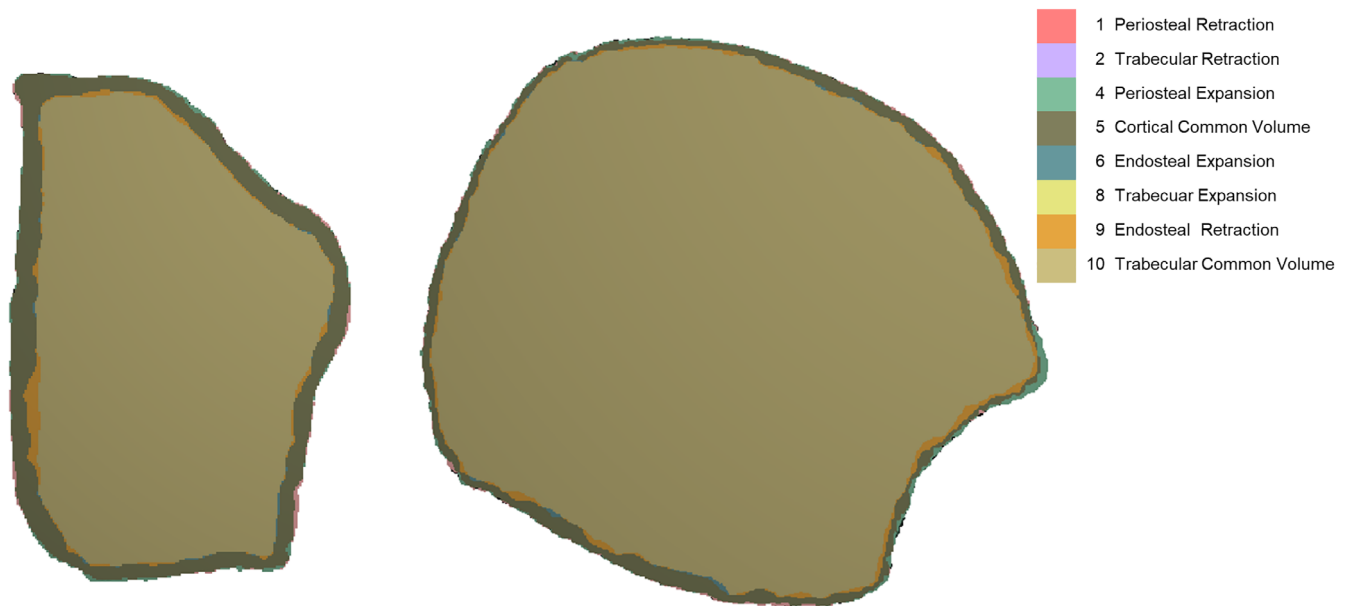
Fig 5. Compartment mask overlay images of the case shown in Fig. 4. The colors indicate the regions used for the calculation of the different indices.

up to 39% (Table 3). For the tibia, the reduction was limited to 8%. Relaxing this threshold to 40% obviously increased the number of participants, in particular for the female, while increasing it to 60% would further reduce the number of scans (Appendix A).

An example of a cross-sectional image at BL and 7 years FU for a typical female case is shown in Fig. 4, for both the tibia and radius. It can be observed that the automatically created endosteal contour retracts due to the trabecularization of the cortical bone. It can also be observed that the trabecular architecture is well recognizable, even after 7 years, while cortical porosity is increased. The corresponding compartment mask overlay image, from which the periosteal/endosteal expansion/retraction parameters are calculated, is shown in Fig. 5.

Table 4. Mean Values With Standard Deviations (SD) for Periosteal and Endosteal Expansion and Retraction Distances, in Microns, for the Radius and Tibia in Female and Male Measured at 3.5 and 7 Years for the Case Where the Threshold for the Overlap was Set to 50%

	Female				Male			
	3.5 years		7 years		3.5 years		7 years	
Radius *n*	135		130		49		43	
Per.Exp	*36.6*	(13.3)	*34.7*	(19.0)	40.0	(16.6)	35.3	(13.4)
Per.Ret	34.3	(13.4)	**37.3**	(17.1)	36.6	(16.3)	**40.6**	(19.8)
End.Ret	**67.1***	(32.6)	**96.8***	(52.5)	**52.6***	(19.4)	**58.8***	(28.9)
End.Exp	*29.1**	(14.3)	*26.5**	(17.2)	39.2*	(19.9)	40.5*	(24.4)
Tb.Exp	0.0*	(0.2)	0.1*	(1.1)	**0.1***	(0.3)	**0.0***	(0.0)
Tb.Ret	0.0	(0.1)	0.1	(0.3)	0.1	(0.3)	0.0	(0.1)
Net.Per.Exp	*2.4*	(22.6)	*−2.5*	(29.7)	3.4	(26.7)	−5.3	(27.9)
Net.End.Exp	***−38.0***	(41.0)	***−70.4* **	(63.0)	−13.3*	(32.5)	−18.2*	(44.2)
Tibia *n*	215		218		53		53	
Per.Exp	**45.9**	(19.4)	**45.9**	(21.7)	**44.4**	(15.2)	**44.8**	(21.9)
Per.Ret	*33.2*	(16.7)	*37.3*	(21.2)	35.6	(19.1)	**43.9**	(21.1)
End.Ret	**77.7**	(35.0)	**105.5 ***	(61.0)	**68.5**	(31.4)	**80.9 ***	(57.3)
End.Exp	*39.4**	(22.7)	*35.0**	(22.6)	44.9*	(14.7)	54.6*	(26.6)
Tb.Exp	**0.1**	(0.4)	**0.2**	(0.8)	**0.0**	(0.1)	**0.0**	(0.1)
Tb.Ret	0.0	(0.1)	0.0*	(0.1)	**0.1**	(0.5)	**0.0***	(0.1)
Net.Per.Exp	**12.8**	(21.1)	8.8	(36.5)	**8.7**	(23.8)	1.0	(33.0)
Net.End.Exp	***−38.4***	(42.4)	***−70.8 * **	(74.1)	−23.5*	(35.9)	−26.3*	(71.3)

Bold values are significantly different from the sensitivity study population (Kruskal–Wallis, *p* < 0.05); asterisks indicate significant differences between male and female (Kruskal–Wallis, *p* < .05); and italic values indicate significant changes between the two time points (Wilcoxon, *p* < .05).

For the subjects with at least a 50% overlap, the radius average (SD) LCH consisted of 86 (11) slices and 86 (9) slices for the females and males, respectively, corresponding to 78% (11%) and 78% (10%) of the BL volume, respectively. For the tibia, these numbers were 96 (7) slices and 93 (9) slices for the females and males, respectively, corresponding to 88% (7%) and 85% (8%) of the BL volume, respectively. The average periosteal and endosteal expansion and retraction distances are listed in Table 4, and the average net periosteal and endosteal expansion and retraction distances are also displayed in Fig. 6.

For the radius, a significant Per.Ret was found only at 7 years for females and males (Table 4). Because this was largely compensated by periosteal expansion, this did not result in a significant negative Net.Per.Exp (Fig. 6). A significant and large End.Ret was found for females and males that was only partly compensated by End.Exp. For the females only, this resulted in a significant negative Net.End.Exp at both time points that further decreased over time. At both time points, the Net.End.Exp in females was significantly different from that in males.

For the tibia, significant Per.Exp was found at both time points for both females and males, but this was largely compensated by Per.Ret, leaving a significant but small Net.Per.Exp only at 3.5 years that was reduced and no longer significant at 7 years. As for the radius, a large and significant End.Ret was found that was only partly compensated by End.Exp. For the females only, this resulted in a significant negative Net.End.Exp at both time points that further decreased over time. At both time points, the Net.End.Exp in females was significantly different from that in males.

When reducing the percentage overlap threshold to 40%, or increasing it to 60%, the results only slightly changed (Appendix A). In all cases, a significant negative Net.End.Exp was found at both time points in females only, while a significant but small Net.Per.Exp was detected only for the tibia and only at 3.5 years.

Results of the standard cortical parameters calculated for the full images (110 slices) without registration were available at all time points for the radius for 195 females and 53 males and for the tibia for 221 females and 54 males (Table 5). The results demonstrate no significant change in Tt.V for the radius and a significant but minor (0.33%) increase for the female tibia only at 7 years. A significant increase in Tb.V was found for the females only, at the radius at 7 years only, and at the tibia at both time points. A significant reduction of Ct.V and Ct.Th was found for the females at both 3.5 years and 7 years for both radius and tibia. For the males, a significant reduction of Ct.V was found only at the tibia at 7 years, while no significant reduction of Ct.Th was found.

The changes in Ct.Th found can be related to the expansion/retraction results as they should be comparable to the Net.Per. Exp + Net.End.Exp. For the females, the change in Ct.Th (−65 microns) at the radius at 7 years FU compares well with the Net.Per.Exp + Net.End.Exp (−72.9 microns). Also for the tibia, the change in Ct.Th (−50 microns) compares well to the Net. Per.Exp + Net.End.Exp (−62 microns).

Discussion

The first goal of this study was to test the sensitivity and reproducibility of the newly developed 3D registration approach for detecting changes in the bone compartments. The least significant change in the net periosteal/endosteal expansion/retraction parameters introduced here when tested on data from an earlier reproducibility study was better than 43 microns at the radius and 26 microns at the tibia, and was relatively independent of the method used for contouring. These distances are much less than the voxel size of the images (82 microns), which is possible because they represent the average expansion/retraction. In reality, the expansion/retraction is not uniform, as can be
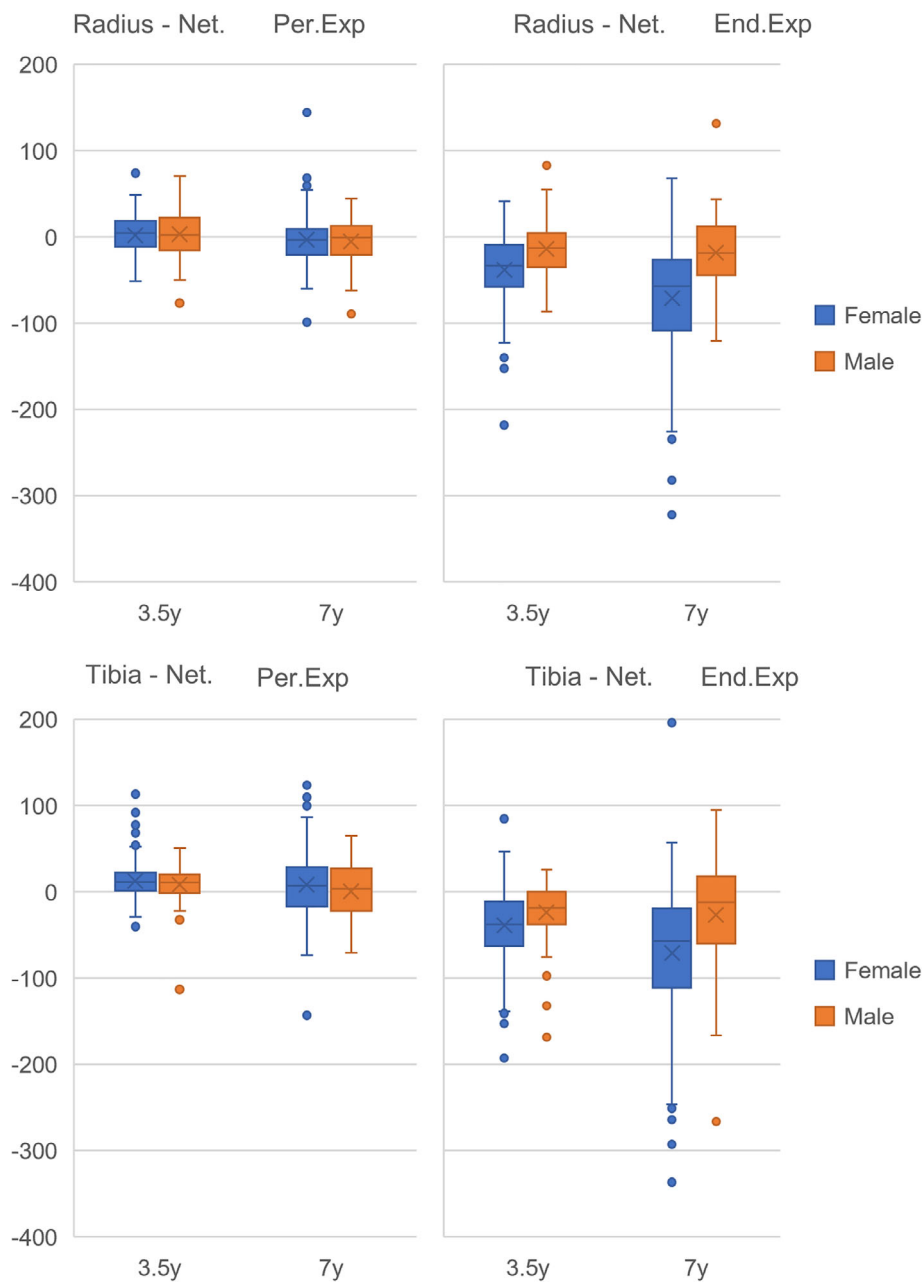
Fig 6. The net periosteal expansion (left) and net endosteal expansion (right) for the radius (top) and tibia (bottom) for females (blue) and males (orange) at 3.5 and 7 years. The mean is indicated by the cross. For the radius, the Kruskal–Wallis test indicated a significant negative Net.End.Exp for females at 3.5 and 7 years (both $p < .001$) and significant differences between males and females at 3.5 years ($p = .011$) and 7 years ($p < .001$). The Wilcoxon test indicated significant differences between both time points for Net.Per.Exp ($p = .041$) and Net.End.Exp in females ($p < .001$). For the tibia, the Kruskal–Wallis test indicated a significant but small Net.Per.Exp only at 3.5 years for females ($p = .009$) and males ($p = .039$). A significant negative Net.End.Exp was found only for females at 3.5 and 7 years (both $p < .001$) and a significant difference in Net.End.Exp was found between females and males at 3.5 years ($p = .011$) and 7 years ($p < .001$). The Wilcoxon test indicated significant differences between both time points for Net.End.Exp in females ($p < .001$).

observed in Fig. 5 and from the fact that both expansion and retraction are reported for the periosteal/endosteal contours. This indicates that the contours shift over at least 1 voxel in the outward direction at some locations and in the inward direction at other locations. At the periosteal surface, this can be related to manual corrections of the contours (in the case of the snake algorithm), movement artifacts, and image noise. At the endosteal side, no manual corrections were applied in this study, but the automated contouring algorithm is sensitive to noise and movement artifacts as well. Furthermore, registration errors potentially can result in unrealistic expansion/retraction values for periosteal/endosteal expansion/retraction parameters. The

Table 5. Results for the Standard Cortical Parameters Calculated for the Full Images (110 Slices)

	Female (n = 195)						Male (n = 53)					
	Baseline		3.5 years		7 years		Baseline		3.5 years		7 years	
Radius n	195		195		195		53		53		53	
Tt.V	2355	(409)	2344	(420)	2353	(413)	3332	(599)	3298	(597)	3316	(574)
Tb.V	1909	(409)	1905	(423)	1940**	(416)	2687	(602)	2642	(603)	2679	(580)
Ct.V	472	(76)	461**	(76)	436**	(77)	679	(108)	687	(115)	669	(118)
Ct.Th	0.851	(0.16)	0.834**	(0.16)	0.786**	(0.17)	0.997	(0.19)	1.016	(0.20)	0.987	(0.20)
Tibia n	221		221		221		54		54		54	
Tt.V	6389	(1003)	6391	(1006)	6410**	(1012)	8084	(1265)	8093	(1271)	8091	(1270)
Tb.V	5499	(1034)	5510*	(1053)	5571**	(1054)	6830	(1329)	6855	(1338)	6863	(1340)
Ct.V	934	(148)	915**	(146)	882**	(144)	1309	(206)	1292	(198)	1281**	(196)
Ct.Th	1.090	(0.21)	1.075**	(0.20)	1.040**	(0.21)	1.330	(0.27)	1.323	(0.27)	1.309	(0.27)

Shown are the average values and the standard deviation between brackets.
Significantly different from baseline (Friedman): *$p < .05$; **$p < .01$.

Net.Per.Exp and Net.End.Exp parameters are less sensitive for such registration errors because the expansion resulting from 3D registration errors is compensated for by the resulting retraction at other locations. In severe cases, however, 3D registration errors may affect the calculation of the LCH and thus affect the results for all parameters. Better sensitivity is found, in general, for the tibia than for the radius. This is in agreement with the general observation that measurements at the radius are less precise than at the tibia in particular in the cortical region,[27,33] which relates to the fact that movement artifacts at the tibia are generally lower and that the tibia and its cortical area are larger.

The rationale for not making any manual corrections at the endosteal contour is that, in contrast to the periosteal side, such manual corrections are rather subjective and operator dependent. The results for outliers were visually checked to investigate if these were the result of contour errors, but in none of these cases the contours were obviously wrong. Typically, these were cases with a very porous cortex, almost appearing as a double cortex at some slices, where the algorithm may switch between the inner and outer cortex even within one slice. In most of these cases, corrections would have been made by an operator to straighten out the endosteal contour, but as the definition of a cortex layer in these situations is very challenging, it is likely that the reproducibility of such corrections is poor, in particular for these cases. Although the automated contouring algorithm used thus may not always identify the endosteal contour in the same way as an operator, at least the results are reproducible (assuming good image quality). Whereas manual corrections may have reduced such outliers, it may also reduce the sensitivity to detect such changes.

In contrast to the endosteal contours, the periosteal contours that were generated using the snake algorithm (part of the standard workflow) were potentially manually corrected. No information was available with regard to if corrections were made. Although such corrections could have resulted in larger reproducibility errors, the values found here are assumed to be representable for clinical practice. Contours made using the autocontouring generally are a bit smoother than those of the snake algorithm. Nevertheless, differences in LSC between the snake algorithm and the autocontouring algorithm were found to be minor (<2.9 microns) (Table 2). It should be noted that small differences (<1 micron) are found as well for the endosteal expansion/retraction parameters, even though the endosteal contour was automatically generated in both cases. These small differences relate to the fact that the LCH can differ by one slice depending on the periosteal contouring method.

When using the full-height stacks (110 slices) rather than the LCH after 3D registration, the quantification of the LSC for the net periosteal/endosteal expansion (here noted as Net.Per.Exp* and Net.End.Exp*) was found to be some 5 to 10 times higher. This demonstrates that the 3D LCH approach is needed to reach the required sensitivity for detecting subtle changes over time. Potentially, the area matching approach can also reduce these errors. In the present study, this was not investigated because, as explained in the introduction, this approach is expected to obscure any periosteal expansion/retraction, the detection of which was the main goal of this study. However, as the results indicate little or no expansion/retraction at the periosteal boundary calculating the Net.End.Exp according to Eq. 4 should provide adequate results as well if these calculations are limited to the common region defined by the area matching algorithm.

In this study, the quality of the 3D registration was quantified by the percentage overlap within the LCV of the images. This differs from image correlation coefficients used in other studies.[34] The reason for using the percentage overlap rather than a correlation is because it eases the interpretation and because the correlation coefficient does not differentiate well in case the overlap is good to perfect. The percentage overlap for the images used in the sensitivity study was at least 48% for the radius and 59% for the tibia. The maximum overlap found for any images was 74% at the radius and 80% at the tibia. The fact that these numbers are not higher relates to the fact that this overlap was calculated only for the trabecular region and that, at the 82-micron resolution, most voxels are at the surface of trabeculae. Whether a voxel at the surface exceeds the threshold for segmentation of bone tissue depends on the exact sub-voxel positioning, making it an almost random event. From visual inspection, however, it was found that these numbers indicated good 3D registration.

A second goal was to assess differences in periosteal/endosteal expansion over time between men and women in a cohort of subjects during normal aging after retirement. Results of the cohort study showed a significant net endosteal retraction at both radius and tibia after 3.5 years that is further increased at 7 years for females, whereas in males no significant endosteal retraction was found (Table 4). Significant periosteal expansion was found only for the tibia at 3.5 years, but this was much smaller (12.8 microns in females and 8.7 microns in males) than the endosteal retraction (−38.4 microns in females and −23.5

microns in males) and was no longer significant at 7 years. In fact, although significant only at the female radius, there was a trend to net periosteal retraction over time. Whereas the results for the females are as expected, the lack of any sign of periosteal expansion in males was not. To make sure this finding is not related to the 3D registration procedure and the use of the LCH region, we also performed the HR-pQCT advanced cortical evaluation for the full-stack height as used in many earlier studies. These results supported our findings. For females and males, no significant change in Tt.V (ie, periosteal expansion) was found, with the exception of one minor (0.33%) reduction at 7 years for the tibia in females, while a significant increase in Tb.V (ie, cortical endosteal retraction) was found for the females. Although the change in Ct.Th did not correspond exactly to the calculated Net.Per.Exp + Net.End.Exp, such differences can be explained by differences in the analyzed region (110 slices versus LCH), the use of a slightly different periosteal contour that is used by default in the advanced cortical evaluation and differences in the included subjects. Taken together, these results consistently indicate that the bone periosteal boundary is no longer expanding in this age group, while the cortical endosteal boundary is retracting, but much more in females than in males. This may be one of the factors that explains differences in bone fragility development between females and males at this age.

In this study, the trabecular expansion (Tb.Exp) and trabecular retraction (Tb.Ret) parameters were expected to be very small, and the results indeed indicate that these could easily be ignored as their values are negligible. This would enable the calculation of the Net.Per.Exp in a more intuitive manner as Per.Exp – Per.Ret and the Net.End.Exp as End.Exp – End.Ret. In other situations, however, these parameters may play a more relevant role. For example, in case of very thin cortices or in case of radial expansion due to growth, these parameters need to be considered to correctly calculate the net periosteal and endosteal expansion.

The quality of the registration was based on the %OL of the segmented tissue between the FU and BL image within the LCV and a 50% threshold for inclusion was used based on the results of the sensitivity study. There are several arguments, however, for lowering this threshold. First, for this cohort study, the 50% threshold resulted in the exclusion of a substantial number of scans, in particular for the female radii. When comparing the baseline characteristics for female radii for which one of the two follow-up scans was excluded, it was found that this partly excluded group had a significant lower trabecular density and trabecular thickness than the group for which no measurements were excluded, while total density, cortical density, cortical thickness, trabecular number, and trabecular separation did not differ significantly (Kruskal–Wallis, $p < 0.05$). For the group for which both follow-up scans were excluded, in addition a significant lower total density was found. These results indicate that the 50% overlap may bias the data set as subjects with lower trabecular density and thickness are more likely to be excluded. Second, it can be argued that the %OL values obtained from the sensitivity study that involved younger adults cannot be directly translated to the older/postmenopausal subjects of the cohort study, as the younger subjects will have a higher bone density and thicker trabecula, which will increase the %OL. Third, bone remodeling that is expected to occur within several years will also reduce the %OL, even in case the 3D registration would be perfect. Finally, none of the conclusions nor the significance of the Net.Per.Exp and Net.End.Exp values changed when lowering the threshold to 40% overlap, whereas for the other parameters only female Per.Ret at 3.5 years changed to significant. Taken together, this suggests that a 40% overlap threshold would be preferred in case of longitudinal studies in elderly, in particular if the 50% results in a large number of exclusions. An alternative approach that potentially could reduce the loss of inclusions would be to set this threshold such that it would maximize the sensitivity for detecting changes over time or between groups.

The use of the LCH will reduce the size of the region that can be analyzed compared with the full-height stack of 110 slices (corresponding to 9.0 mm). For the radius, the LCH was 86 slices (corresponding to 7 mm or 78% of the BL volume), whereas for the tibia it was between 93 and 96 slices (corresponding to 7.63 and 7.87 mm or 85% and 88% of the BL volume, respectively). Typically, the most distal and/or the most proximal regions are lost. In the present study, no scans were excluded because of a limited LCH height as such height reductions are merely due to (small) positioning errors during scanning and do not represent issues with the 3D registration or images. When using the area matching approach, it has been recommended that a minimum of 75% volumetric overlap is required (although no justification for this number was provided).[25] However, this number cannot be directly translated to a minimum LCH volumetric overlap or height, as the LCH on average will be smaller than the remaining stack height when using the slice matching (eg, for the female radius in this study, the common region based on area matching was 89%). Based on the average minus 2 times SD, one could recommend a lower limit of around 65 slices (or 57% of the BL volume) for the radius and 75 slices (or 69% of BL volume) for the tibia without compromising the number of included scans too much. However, smaller volumes may be acceptable as well in case it is reasonable to assume that parameters are changing uniformly throughout the scanned volume.

The expansion/retraction rates found here are much less than those reported in earlier studies. The net periosteal retraction found here for the radius in females was 10 microns per year, which is much less than the value of 58 microns per year reported in an earlier study for postmenopausal women in a similar age range.[6] In that earlier study, a net periosteal expansion of 8 microns per year was reported for the radius, whereas in this study no significant net periosteal expansion was found. Also, for men the endosteal retraction rate at the radius found here (2.6 microns per year) is much less than the 20 microns per year reported in an earlier study for men in a similar age range.[20] In that earlier study, a periosteal expansion rate of 10 microns per year was reported, while, again, in this study, no periosteal expansion was found for the radius. Such differences between results of earlier studies potentially can be due to differences in measurement site (one-third radius in the earlier studies, distal radius in this study) but likely also relate to differences in imaging technology used (dual-energy X-ray absorptiometry [DXA] in the earlier study and HR-pQCT here). Because of its projective nature, the DXA measurements tend to represent the local maximum expansion in the projected view, whereas in this study any local periosteal expansion is smeared out over the full periosteal bone surface. Another potential explanation for this difference would be that HR-pQCT is less sensitive to detect changes in the periosteal contour than DXA, eg, in case periosteal apposition would be less mineralized, not reaching the threshold set in HR-pQCT scanning. This, however, seems unlikely, as significant and substantial Per.Exp and Per.Ret are found in several cases. But, as these amounts are similar, no significant Net.Per. Exp results.

Some limitations of the present study should be mentioned as well. First, only the average Net.End.Exp in females reaches values that clearly exceed the LSC, whereas for males these

values are close to the LSC. This indicates that the possibilities to detect expansion/retraction in individual patients are limited. When studying a cohort, however, significant changes smaller than the LSC can be studied. Second, the sensitivity study to determine the LSC was performed only for females that are known to have smaller bones than males and that were younger (21 to 47 years) than the subjects of the cohort study (65 to 72 years). As we look for differences between repeated measurements, and because the measurements are corrected for bone size, it seems reasonable to assume the same LSC values are also valid for males. As also discussed above, however, it is possible that the LSC values for these younger adults cannot be directly translated to the older/postmenopausal subjects of the cohort study. Finally, the present approach only detects the average smeared-out endosteal retraction, whereas in fact this might consist of a few large local spots instead of a uniform retraction. It would be straightforward to further quantify this bone loss pattern by extracting the End.Ret regions from the compartment mask overlay images (Fig. 5) and, eg, perform a component labeling and distance transformation analysis on these to count the number of spots and their size.

Strong points of this study are the accurate 3D registration of BL and FU images to get the LCH that is common for all three time points. Without this approach, the sensitivity for detecting periosteal/endosteal expansion would be very low, as was shown in the sensitivity study. Furthermore, the results obtained here are much more detailed than available from more standard cortical evaluations. Finally, although in the present study we focus on the quantitative determination of periosteal/endosteal expansion, the use of the 3D registration also enables the placement of the BL contours exactly on FU images. In this way, it is possible also to get a very detailed qualitative picture about changes in bone geometry. The major advantage of the present approach, however, is the fact that it will increase the sensitivity for detecting cortical changes. In addition, the 3D registration approach used here that only takes the cancellous bone region into account potentially may also improve the sensitivity for detecting trabecular bone changes compared with 3D registration methods that use the full stack for 3D registration. This increased sensitivity makes it possible to get significant results within the time period of a clinical follow-up study (as demonstrated here) but may also allow for the reduction in number of participants in clinical studies.

In conclusion, the results obtained here demonstrate that it is possible to measure changes in endosteal contours in longitudinal studies within several years. For the cohort of elderly just after retirement as investigated here, no significant periosteal expansion is found at 7 years follow-up, while there is significant endosteal retraction in females but not in males. Whether these changes in cortical geometry are related to fracture risk remains to be investigated in larger cohorts.

Disclosures

BvR is a consultant for Scanco Medical AG. EB is a consultant for Nestlé and has received speaker fees from Labatec outside the submitted work. KI is contracted as CSO for NC Biomatrix BV. TC, RC, and SF have nothing to disclose.

Acknowledgments

Authors' roles: Conceptualization and investigation: BvR, EB, TC, RC, and SF. Data curation and formal analysis: BvR, EB, and TC. Methodology, software, project administration, validation, visualization, and writing—original draft preparation: BvR. Resources: EB, TC, KI, RC, and SF. Supervision: KI. Writing—review and editing: EB, TC, KI, RC, and SF.

Author contributions: BvR: Conceptualization; data curation; formal analysis; investigation; methodology; project administration; software; validation; visualization; writing-original draft. EB: Conceptualization; data curation; formal analysis; investigation; resources; writing-review & editing. TC: Conceptualization; data curation; formal analysis; investigation; resources; writing-review & editing. KI: Resources; supervision; writing-review & editing. RC: Conceptualization; investigation; resources; writing-review & editing. SF: Conceptualization; investigation; resources; writing-review & editing.

Data availability statement

The data that support the findings of this study are available from the corresponding author upon reasonable request.

References

1. Ruff CB, Hayes WC. Sex differences in age-related remodeling of the femur and tibia. J Orthop Res. 1988;6(6):886-896.

2. Garn SM, Sullivan TV, Decker SA, Larkin FA, Hawthorne VM. Continuing bone expansion and increasing bone loss over a two-decade period in men and women from a total community sample. Am J Hum Biol. 1992;4(1):57-67.

3. Bouxsein ML, Myburgh KH, van der Meulen MC, Lindenberger E, Marcus R. Age-related differences in cross-sectional geometry of the forearm bones in healthy women. Calcif Tissue Int. 1994;54(2):113-118.

4. Seeman E. During aging, men lose less bone than women because they gain more periosteal bone, not because they resorb less endosteal bone. Calcif Tissue Int. 2001;69(4):205-208.

5. Ramchand SK, Seeman E. The influence of cortical porosity on the strength of bone during growth and advancing age. Curr Osteoporos Rep. 2018;16(5):561-572.

6. Szulc P, Seeman E, Duboeuf F, Sornay-Rendu E, Delmas PD. Bone fragility: failure of periosteal apposition to compensate for increased endocortical resorption in postmenopausal women. J Bone Miner Res. 2006;21(12):1856-1863.

7. Aeberli D, Schett G. Cortical remodeling during menopause, rheumatoid arthritis, glucocorticoid and bisphosphonate therapy. Arthritis Res Ther. 2013;15(2):208.

8. Tournis S, Samdanis V, Psarelis S, et al. Effect of rheumatoid arthritis on volumetric bone mineral density and bone geometry, assessed by peripheral quantitative computed tomography in postmenopausal women treated with bisphosphonates. J Rheumatol. 2012;39(6):1215-1220.

9. Zhu TY, Griffith JF, Qin L, et al. Alterations of bone density, microstructure, and strength of the distal radius in male patients with rheumatoid arthritis: a case-control study with HR-pQCT. J Bone Miner Res. 2014;29(9):2118-2129.

10. di Leo C, Bestetti A, Bastagli A, et al. Geometry and bone mass in primary hyperparathyroidism assessed by peripheral quantitative computed tomography (pQCT). Radiol Med. 2003;105(3):171-179.

11. Bala Y, Chapurlat R, Cheung AM, et al. Risedronate slows or partly reverses cortical and trabecular microarchitectural deterioration in postmenopausal women. J Bone Miner Res. 2014;29(2):380-388.

12. Deeks ED. Denosumab: a review in postmenopausal osteoporosis. Drugs Aging. 2018;35(2):163-173.

13. Seeman E, Delmas PD, Hanley DA, et al. Microarchitectural deterioration of cortical and trabecular bone: differing effects of denosumab and alendronate. J Bone Miner Res. 2010;25(8):1886-1894.

14. Zebaze RM, Libanati C, Austin M, et al. Differing effects of denosumab and alendronate on cortical and trabecular bone. Bone. 2014;59: 173-179.

15. Chavassieux P, Chapurlat R, Portero-Muzy N, et al. Bone-forming and antiresorptive effects of romosozumab in postmenopausal women with osteoporosis: bone histomorphometry and microcomputed tomography analysis after 2 and 12 months of treatment. J Bone Miner Res. 2019;34(9):1597-1608.

16. Lindsay R, Zhou H, Cosman F, Nieves J, Dempster DW, Hodsman AB. Effects of a one-month treatment with PTH(1-34) on bone formation on cancellous, endocortical, and periosteal surfaces of the human ilium. J Bone Miner Res. 2007;22(4):495-502.

17. Lindsay R, Krege JH, Marin F, Jin L, Stepan JJ. Teriparatide for osteoporosis: importance of the full course. Osteoporos Int. 2016;27(8): 2395-2410.

18. Hansen S, Hauge EM, Beck Jensen JE, Brixen K. Differing effects of PTH 1-34, PTH 1-84, and zoledronic acid on bone microarchitecture and estimated strength in postmenopausal women with osteoporosis: an 18-month open-labeled observational study using HR-pQCT. J Bone Miner Res. 2013;28(4):736-745.

19. Dempster DW, Zhou H, Ruff VA, Melby TE, Alam J, Taylor KA. Longitudinal effects of teriparatide or zoledronic acid on bone modeling- and remodeling-based formation in the SHOTZ study. J Bone Miner Res. 2018;33(4):627-633.

20. Szulc P, Delmas PD. Bone loss in elderly men: increased endosteal bone loss and stable periosteal apposition. The prospective MINOS study. Osteoporos Int. 2007;18(4):495-503.

21. Boutroy S, Bouxsein ML, Munoz F, Delmas PD. In vivo assessment of trabecular bone microarchitecture by high-resolution peripheral quantitative computed tomography. J Clin Endocrinol Metab. 2005; 90(12):6508-6515.

22. Manske SL, Zhu Y, Sandino C, Boyd SK. Human trabecular bone microarchitecture can be assessed independently of density with second generation HR-pQCT. Bone. 2015;79:213-221.

23. Buie HR, Campbell GM, Klinck RJ, MacNeil JA, Boyd SK. Automatic segmentation of cortical and trabecular compartments based on a dual threshold technique for in vivo micro-CT bone analysis. Bone. 2007;41(4):505-515.

24. Burghardt AJ, Buie HR, Laib A, Majumdar S, Boyd SK. Reproducibility of direct quantitative measures of cortical bone microarchitecture of the distal radius and tibia by HR-pQCT. Bone. 2010;47(3):519-528. https://doi.org/10.1016/j.bone.2010.05.034.

25. Whittier DE, Boyd SK, Burghardt AJ, et al. Guidelines for the assessment of bone density and microarchitecture in vivo using high-resolution peripheral quantitative computed tomography. Osteoporos Int. 2020;31(9):1607-1627.

26. Nishiyama KK, Campbell GM, Klinck RJ, Boyd SK. Reproducibility of bone micro-architecture measurements in rodents by in vivo micro-computed tomography is maximized with three-dimensional image registration. Bone. 2010;46(1):155-161.

27. Ellouz R, Chapurlat R, van Rietbergen B, Christen P, Pialat JB, Boutroy S. Challenges in longitudinal measurements with HR-pQCT: evaluation of a 3D registration method to improve bone microarchitecture and strength measurement reproducibility. Bone. 2014;63: 147-157.

28. Kemp TD, de Bakker CMJ, Gabel L, et al. Longitudinal bone microarchitectural changes are best detected using image registration. Osteoporos Int. 2020;31(10):1995-2005.

29. Kawalilak CE, Johnston JD, Olszynski WP, Kontulainen SA. Least significant changes and monitoring time intervals for high-resolution pQCT-derived bone outcomes in postmenopausal women. J Musculoskelet Neuronal Interact. 2015;15(2):190-196.

30. Glüer CC, Blake G, Lu Y, Blunt BA, Jergas M, Genant HK. Accurate assessment of precision errors: how to measure the reproducibility of bone densitometry techniques. Osteoporos Int. 1995;5(4):262-270.

31. Bonnick SL, Johnston CC Jr, Kleerekoper M, et al. Importance of precision in bone density measurements. J Clin Densitom. 2001;4(2): 105-110.

32. Biver E, Durosier-Izart C, Chevalley T, van Rietbergen B, Rizzoli R, Ferrari S. Evaluation of radius microstructure and areal bone mineral density improves fracture prediction in postmenopausal women. J Bone Miner Res. 2018;33(2):328-337.

33. Macneil JA, Boyd SK. Bone strength at the distal radius can be estimated from high-resolution peripheral quantitative computed tomography and the finite element method. Bone. 2008;42(6): 1203-1213.

34. de Jong JJA, Christen P, Plett RM, et al. Feasibility of rigid 3D image registration of high-resolution peripheral quantitative computed tomography images of healing distal radius fractures. PLoS One. 2017;12(7):e0179413.